Assessment of the FE model mesh influence on the mechanical properties identified for cranial bone

Experimental and numerical investigations

Barbara Autuori[*,**]— **Christophe Delille**[**,***]— **Rémi Delille**[**]
Karine Bruyère[*] — **Catherine Masson**[***] — **Pascal Drazetic**[**]

[*] *Biomechanics and Human Modelling Laboratory – LRE_T 32, INRETS-UCBL*
Case 24, 25, Avenue Francois Mitterrand, F-69675 Bron cedex

[**] *Laboratory of Industrial and Human Automation, Mechanics and Computer Science – C.N.R.S. UMR 8530*
Le Mont Houy, F-59313 Valenciennes

[***] *Laboratory of Applied Biomechanics – INRETS-UMRT24*
Boulevard P. Dramard, F-13916 Marseille cedex 20

barbara.autuori@univ-valenciennes.fr

ABSTRACT. *The present study was undertaken to assess the influence of two FE modelling strategies on the identified mechanical properties of cranial bone samples. Two experimental databases were reproduced numerically using the two mesh types. Experimental tests were four-point and cantilever beam bending loadings carried out on fresh as well as embalmed cranial bone samples. Then, the elasto-plastic properties of four bone samples were identified: Young's modulus, Poisson's ratio and yield stress were determined independently using a dichotomy method. Identification results were highly influenced by element type, geometry reconstruction and loading type.*

RÉSUMÉ. *Cette étude a pour but de déterminer l'influence du type de modélisation EF sur les propriétés mécaniques identifiées d'éprouvettes d'os crânien. Des échantillons d'os crânien frais et embaumés ont été chargés en flexion quatre points et poutre-console. Les propriétés élasto-plastiques de quatre de ces échantillons ont été déterminées par une méthode d'identification : le module d'Young, la limite élastique et le module tangent ont été identifiés de manière indépendante par dichotomie. Les propriétés identifiées ont été fortement influencées par le type d'élément utilisé, la méthode de reconstruction géométrique et le type de chargement simulé.*

KEYWORDS: *finite elements, cranial bone, bending tests, mechanical properties, identification.*

MOTS-CLÉS : *éléments finis, os crânien, essais de flexion, propriétés mécaniques, identification.*

REEF – 14/2005. Biomechanics of impact, pages 379 to 395

1. Introduction

Among biomechanics application fields are orthopedic, maxillofacial surgical planning, prosthesis design, and more recently crashworthiness. Head segment is the most commonly studied in the injury risk prevention of road users since this body part is concerned in fatal outcomes. Actually, according to a recent epidemiological study realized in the Rhone department in France between 1995 and 2000 [1], the number of injuries involving the head is the most important concerning dead victims.

In order to improve road user safety, regulation car crashes are reproduced using physical dummies. The assessment of injury risk is based on the measurement of biomechanical criteria on each body segment. The Head Injury Criteria (HIC) is expressed using the linear acceleration computed at the gravity center of the head dummy (JOCE, 1997). Thus, this criteria takes into account the head kinematical behaviour but local mechanical phenomena like brain contact pressure and skull rupture are ignored.

Nowadays, the numerical tools and computational capacity development allow the use of finite element models to reproduce an impact on the whole body or on body parts. Local mechanical parameters such strains and stresses can be used as criteria for a new assessment of injury risk (King *et al.*, 2003, Willinger *et al.*, 2003). Nevertheless, a good numerical simulation of local phenomena during head impact needs a realistic modeling of head anatomy. Besides to being extremely difficult to reconstruct, it also leads to a large model size since the head is constituted by many components (Newman *et al.*, 1999, Kleiven *et al.*, 2002, Canaple *et al.*, 2003).

Among head constituents, the skull ensures the protection of cranial content. Thus bone architecture and mechanical properties modeling should be particularly realistic. However, the skull geometry is characterized by reinforcements and large thickness variation (Ferré *et al.*, 1986, Ferré *et al.*, 1990). Skull shape reconstruction is usually performed using CT scans or 3D pointing device, and surfaces obtained are then meshed with shell or brick elements. 3D elements allow a realistic representation of thickness but require at least three elements along the skull thickness in order to reproduce a correct mechanical behaviour. Reduction of model size can be achieved using shell elements (Willinger *et al.*, 2003, Autuori *et al.*, 2002, Autuori *et al.*, 2003). Nevertheless, existing head finite element models are built on external or internal surface instead of mean surface, and thickness is constant over the structure.

Bone material properties definition included on head finite element models are submitted to high dispersion. Actually, few studies on cranial bone sample properties are available (Delille *et al.*, 2002, Delille *et al.*, 2003, Evans *et al* , 1957, McElhaney *et al.*, 1970, Barber *et al.*, 1970, Hubbard, 1971, Wood, 1971, Schueler *et al.*, 1994) and the range of results is large due to the variability over the tested population. Values obtained are also influenced by samples conservation technique, which depends on material accessibility (Crandall, 1994). Moreover, no data on damage

behaviour are available and only one of these studies (Hubbard, 1971) is carried out using bending loading even thought an impacted skull should be submitted to this loading mode.

The work presented in this paper was carried out to steer users' experimental and numerical choices for biomechanical studies of cranial bone samples. Two sets of cranial bone samples were tested under either four-point or cantilever beam bending quasi-static loadings. Then, numerical simulations were performed, for each set, on two samples showing different geometries. Mechanical properties were determined using an identification method and the element type influence on obtained values was evaluated.

2. Material and methods

2.1. *Experimental investigation*

2.1.1. *Bone samples*

The cranial bone samples used for four-point bending tests came from an unembalmed 80 year-old female donor. Nine samples were taken from the parietal and occipital bones (Fig.1a) and trimmed more accurately using a diamond low speed saw (isomet®). Samples geometry was chosen approximately about 75 mm in length (L) and 10 mm in width (l) to minimize curvature effects (Fig.2). They were re-hydrated and stored until mechanical testing in a physiologic bath.

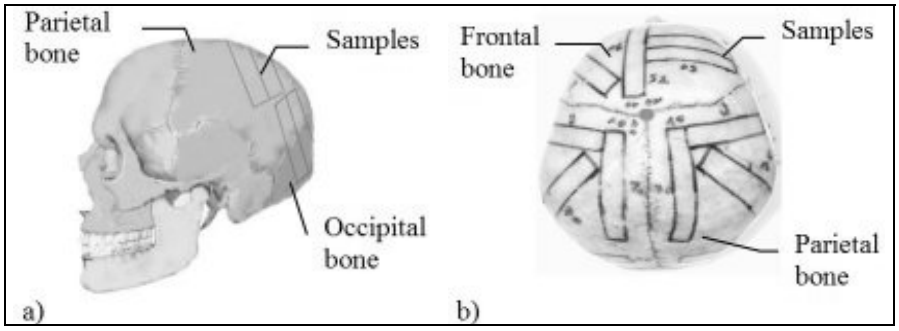

Figure 1. *Bone samples location. a) Four-point bending tests samples : lateral view. b) Cantilever beam tests: top view*

The ten bone samples used for cantilever beam tests were taken from two embalmed male donors who were 83 and 89 year-old. Sampling location was parietal bone (Fig.1b) and geometry obtained using a surgical saw was L =70 mm and l = 13 mm (Fig.2).

Since sandwich material was studied here, samples were not machined and thus sample thickness showed a large variation as it can be observed on the whole skull (Fig.3).

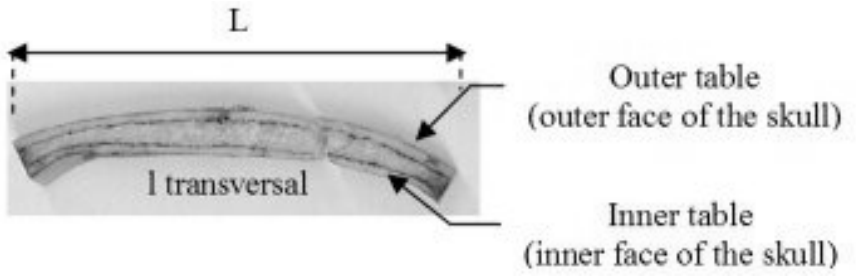

Figure 2. *Sample size*

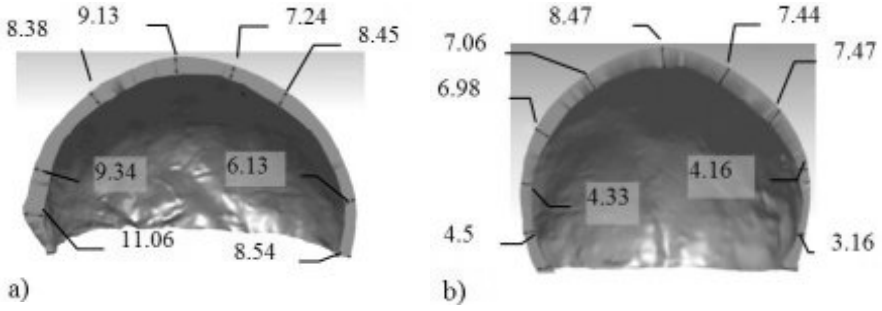

Figure 3. *Thickness distribution over the top of the skull (mm). a) Sagital section cut. b) Coronal section cut*

2.1.2. *Four-point bending tests*

The four-point bending tests were performed using a universal Deltalab® compression machine, with a displacement velocity of 0.3 mm/min. Load was applied to the samples using a mechanical piece made of two cylindrical pieces which were 35 mm apart and had a diameter of 5 mm. This loading piece was fixed to the guided cross member with a free rotation joint (Fig.4a). The sample support was ensured by two cylindrical pieces having a diameter of 5 mm and which formed a span equal to 50 mm. The mechanical tests were carried out up to failure on the sample outer table. The loading machine was equipped with a load cell (TMEF521TC- 500daN) and a global displacement transducer to record force versus displacement curve at the loading piece joint (Fig.4b).

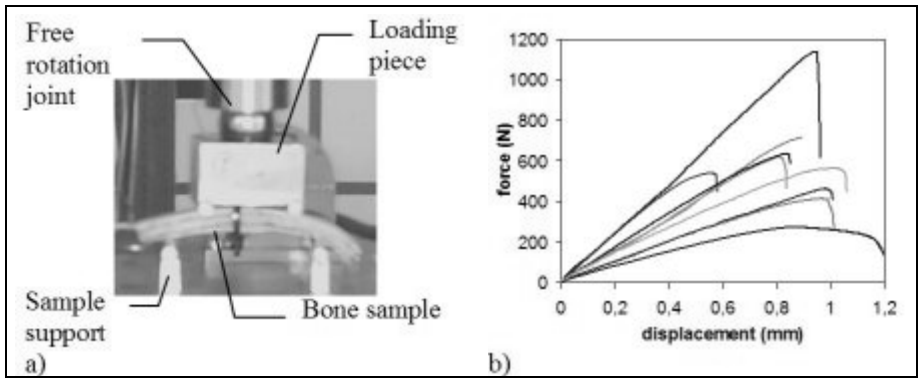

Figure 4. *Four-point bending tests. a) Experimental configuration. b) Experimental force versus displacement curves (n=9)*

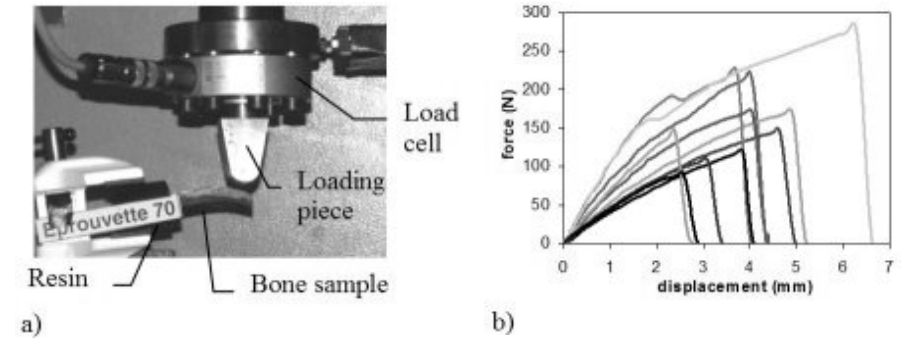

Figure 5. *Cantilever beam bending tests. a) Experimental configuration. b) Experimental force versus displacement curves (n=10)*

2.1.3. *Cantilever beam bending tests*

The cantilever beam bending tests were carried out using a hydraulic guided machine, with a displacement velocity of 40 mm/min. Bone samples were loaded up to failure on the outer table using a twenty millimetres diameter cylindrical piece (Fig.5a). The embedded boundary conditions were provided by a resin block (Axson F1). The force displacement data (Fig.5b) were recorded using a displacement laser cell and a load cell (SY2962-5000N).

2.2. *Simulation of bending tests and material properties identification*

2.2.1. *Geometrical reconstruction and meshing*

Numerical simulations of the two bending tests types described in the previous paragraph were carried out using Abaqus® implicit code. Two samples of each set (Fig.6a-b and 7a-b.) were selected depending on their geometrical complexity (linear and complex) and were meshed distinctly with 4-nodes doubly curved general-purpose shell with finite membrane strains (Koiter-Sanders shell theory) and 6 and 8 nodes (resp. triangular prism and brick) linear solid elements with finite strain and rotation in large-displacement analysis (Hughes-Winget method). Elements size was set to 1 millimetre.

Samples n°1 and n°2 tested using four-point bending loading were assumed to be invariant along the transversal beam section. The sample lateral face was scanned using a two dimensional office scan (Fig.6c). Two distinct shell and solid meshes were realized respectively from the extrusion of the midline curve and of the two dimensional lateral contour (Fig.6d-e). Sample midline curve was used in order to obtain realistic inertial properties. Once the shell mesh was built, real thicknesses of the elements on the lateral border were computed and assigned to the other with respect to the extrusion. Real thickness computation was realised on samples scan (Fig.6c). Segments perpendicular to the element's surface, and going through shell nodes, were created on the 2D scan. The bone boundary was automatically located by the colour change of the pixels along the segment. The element's thickness was computed as the mean value of distances measured on its two nodes on the lateral border.

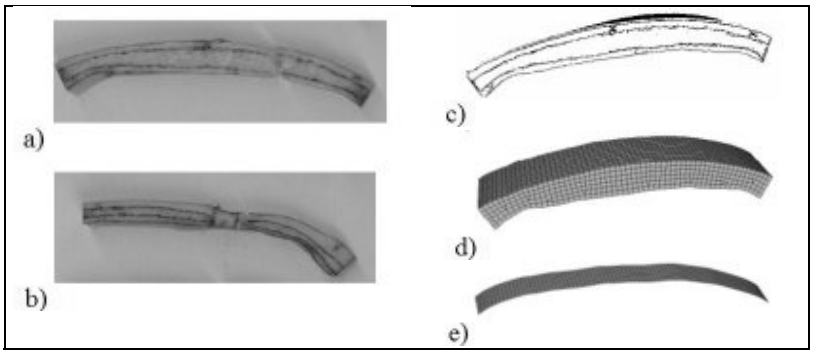

Figure 6. *Reconstruction of bone samples n°1 and 2 tested using four-point bending loading. a) Linear sample geometry (n°1). b) Complex sample geometry (n°2). c) 2D scan of the transversal face (n°1). d) Volumic mesh extruded from the lateral contour. e) Shell mesh extruded from the midline curve*

For samples n°3 and 4 submitted to cantilever beam bending, the real three-dimensional geometry was reconstructed. To achieve this reconstruction, a reproduction of external and internal surfaces was created using resin and modelling clay. Then, the surfaces were digitized using a FaroArm® three-dimensional sensor (Fig.7c). Numerical geometry obtained was smoothed and meshed with brick elements using Hypermesh® (Fig.7d). The shell mesh was realized on the external surface of the sample and elements thickness was measured directly (Fig.7e).

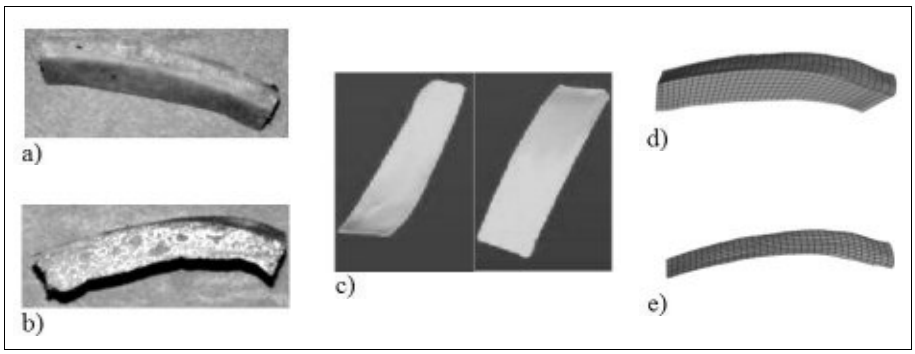

Figure 7. *Reconstruction of bone samples n°3 and 4 tested using cantilever beam bending loading. a) Linear sample geometry (n°3). b) Complex sample geometry (n°4). c) Sample internal and external surfaces (n°3). d) Associate volumic mesh. e) Associate shell mesh*

Moreover, shell mesh physical properties were compared to those obtained using brick elements in order to estimate the mean surface modelling error. Data observed were total mass, gravity centre coordinates and inertia (Table 1). For sample 1 and 2, the shell and brick meshes were geometrically equivalent since their respective mass, gravity centre location and dynamical inertia were corresponding. For sample 3 and 4, some differences were observed.

Table 1. *Differences between shell and full 3D meshes physical properties*

Error (%)	M	xg	yg	zg	I(XX)	I(YY)	I(ZZ)	I(XY)	I(YZ)	I(ZX)
sample 1	*0.52*	*0.12*	*0.01*	*0.58*	*4.46*	*0.39*	*0.62*	*0.41*	*0.06*	*0.03*
sample 2	*1.10*	*0.16*	*0.00*	*2.11*	*3.97*	*1.33*	*1.32*	*1.26*	*0.98*	*0.48*
sample 3	*33.78*	*14.16*	*4.90*	*142*	*31.74*	*117.97*	*31.12*	*53.29*	*204.85*	*238.48*
sample 4	*25.64*	*6.05*	*5.39*	*82.5*	*40.45*	*81.18*	*39*	*18.94*	*115.6*	*111.98*

2.2.2. *Material properties*

We assumed that the bone material was homogeneous, isotropic, with an elastoplastic behaviour defined by Young's modulus E, yield stress σ_e and tangent modulus E'. The Poisson's coefficient ν was chosen equal to 0.21. Young's modulus E was defined by identification of linear part of numerical and experimental force versus displacement curves. Next, plastic properties σ_e and E' were identified. In order to achieve the identification, a first simulation was carried out, using a perfectly plastic behaviour law, a dichotomy method allowed the coincidence of curves to determine σ_e. Then, for the tangent modulus value, the same method allowed the adjustment of experimental curve with the numerical curve obtained using a plastic law, with E and σ_e determined previously.

2.2.3. *Boundary conditions and numerical simulation*

Experimental boundary conditions of four-point bending tests were recorded before tests using a 3D measurement device FaroArm®. Loading piece and support were modelled as rigid analytical surfaces and were guided in displacement with the stabilize option. Low Young's modulus (E = 5 MPa) was assigned to corner elements and fixed displacement conditions were applied to corresponding nodes in order to prevent numerical instability.

For cantilever beam tests, the nodes embedded in resin were fixed. Loading cylinder was modelled as analytical rigid surface and guided in displacement.

Table 2 summarizes the characteristics of samples and experimental bending test simulations: samples identification number, mesh composition, geometrical and physical data.

Table 2. *Samples and simulation characteristics*

		Four points bending		**Cantilever beam bending**	
		Sample 1	*Sample 2*	*Sample 3*	*Sample 4*
Samples size (mm)		*L=75, l=10*		*L=70, l=13*	
Contact surface (mm)		*Diameter =5*		*Diameter =20*	
Number of elements	**shells**	*742*	*682*	*773*	*731*
	bricks	*4120*	*3392*	*4518*	*3922*

2.2.4. *Preliminary study: numerical simulation of simple cases*

Concurrently, simple bending loading cases corresponding to the two experimental tests were modelled in order to compare simulation results, obtained using different element types, to the analytical solution. This preliminary study allowed the evaluation of boundary conditions and samples geometry influence on FE mesh behaviour. To achieve this comparison, linear beams were tested in four-point bending and cantilever beam loading simulations. Firstly, concentrated load (Fig.8) was used, and then, boundary conditions identical to experiments were

applied to these linear beams. Boundary conditions are defined by Figure 8 and finite element mesh definition was the following:

- geometry: 70*15*6 mm^3,
- element size: 1 mm,
- mechanical properties: E=2800 MPa, ν=0.21.

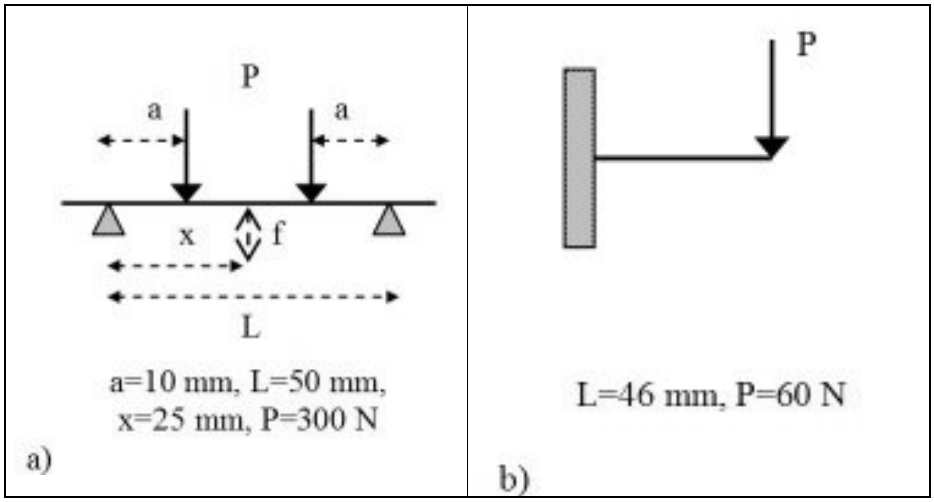

Figure 8. *Preliminary loading configuration. a) Four-point bending. b) Cantilever beam bending*

3. Results

3.1. *Preliminary study results*

3.1.1. *Four-point bending loading*

The comparison of force versus sag displacement curves obtained using analytical solution and finite element simulations showed that the results were equivalent for displacements inferior to 0.2 mm (Fig.9). However, for superior values, the mechanical behaviour of finite element models did not correspond accurately to theoretical solution and was influenced by mesh elements. In this case, linear shell elements represented the best solution with a sag displacement difference of 3.5% compared to theoretical solution (for P=300N), whereas brick elements brought 8.5% for the same value. One can note that the use of specific elements (quadratic shells and reduced integration bricks) did not improve the finite element model response.

Modelling four-point bending test on the same linear beam, using contact interface and spherical joint, confirmed the results obtained above (Fig.10).

Actually, mechanical behaviour of the finite element model meshed using linear brick elements was less stiff than those meshed using shell elements.

Moreover, numerical perturbations were observed on the brick model behaviour (Fig.10). Comparing to results presented above, this demonstrated the influence of contact modelling on bricks elements loaded using four-point bending configuration.

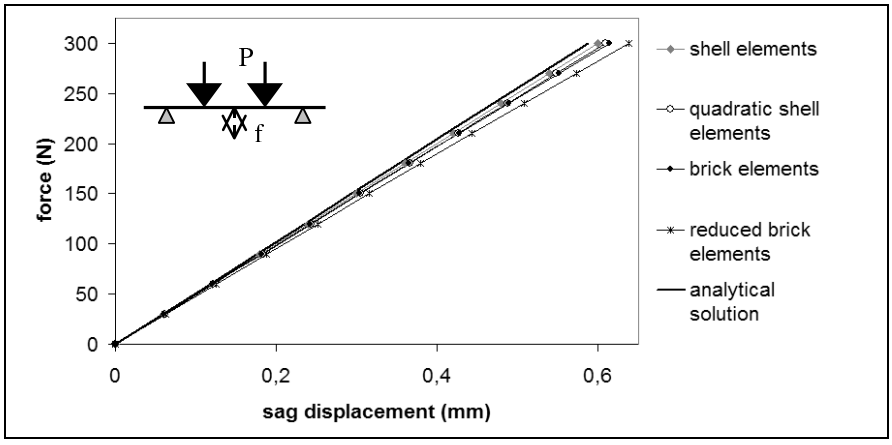

Figure 9. *Four-point bending simulation with concentrated load: force versus sag displacement curve*

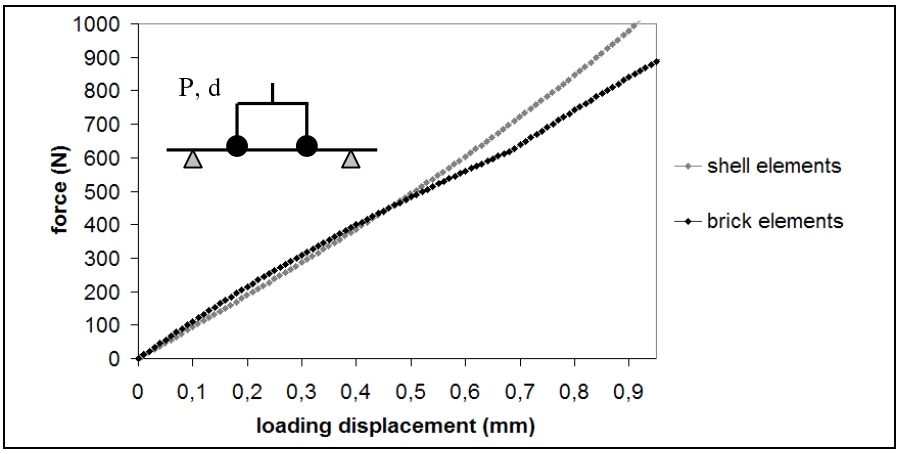

Figure 10. *Four-point bending simulation with contact modelling: force versus loading displacement curve*

3.1.2. *Cantilever beam loading*

For concentrated loading conditions, mechanical behaviour of brick and shell finite element model was equivalent. Actually, curves illustrating force versus sag displacement were totally superposed to analytical solution (results are not illustrated here). When modelling contact interface with an analytical surface, results were equivalent those found with simple loading conditions: shell and brick meshes had the same behaviour (Fig.11).

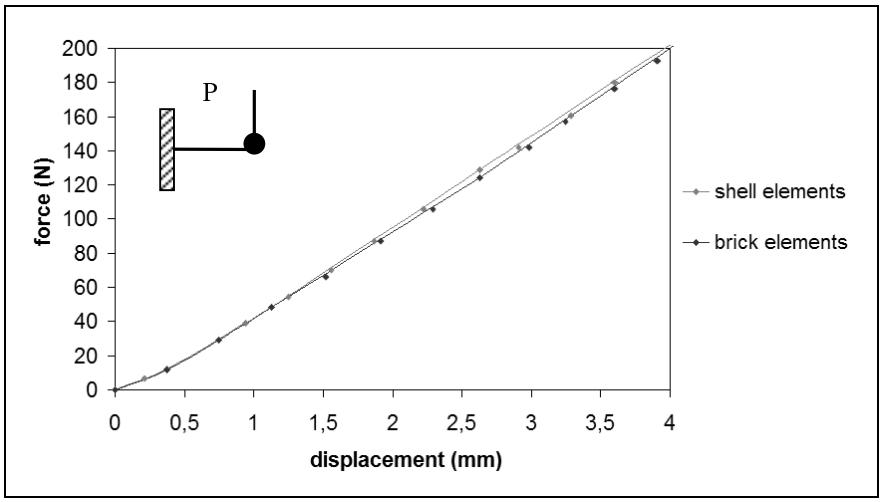

Figure 11. *Cantilever beam bending simulation with contact modelling: force versus loading displacement curve*

3.2. *Identification of bone properties*

Results presented below are experimental and numerical force versus loading displacement curves obtained for each bone sample (n°1 to 4). Identification of material properties was performed as presented in the 2.2.2 paragraph using surface and volume finite element models. Then, values identified using one mesh type (shells or bricks) were introduced in a new simulation performed using the other mesh type. Thus, four simulations were performed for each bending test.

Concerning the sample 1, numerical identification obtained was equivalent for shell and brick mesh (Fig.12). Actually, the two force versus displacement curves fitted the experimental data for same mechanical property values (E= 2600 MPa, σe=20 MPa, E'=2000MPa) (Table 3).

Mechanical properties identified for sample 2 were influenced by the reconstruction type. In fact, finite element model meshed using shells was stiffer: Young's modulus identified with bricks was 58% higher (Table 3). Moreover, the

simulation performed using volume mesh associated to material properties identified using shell finite element model gave error values higher than those performed using the opposite configuration (Fig.13).

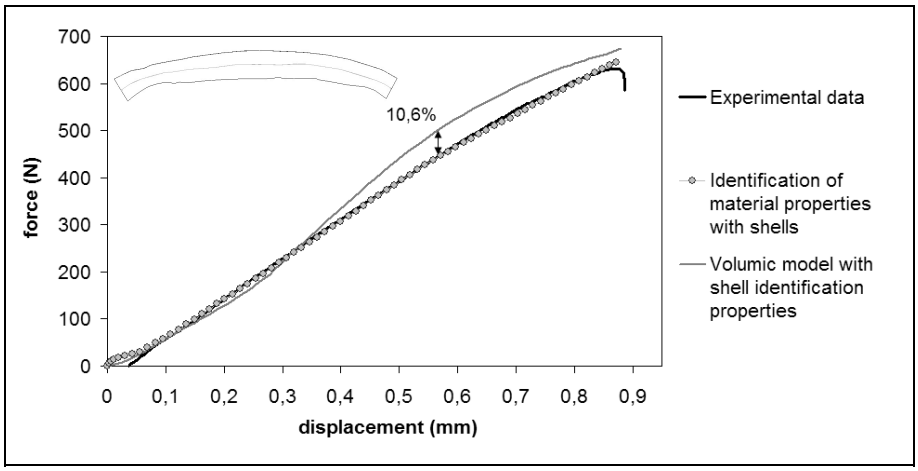

Figure 12. *Experimental and numerical force versus displacement curves for sample 1*

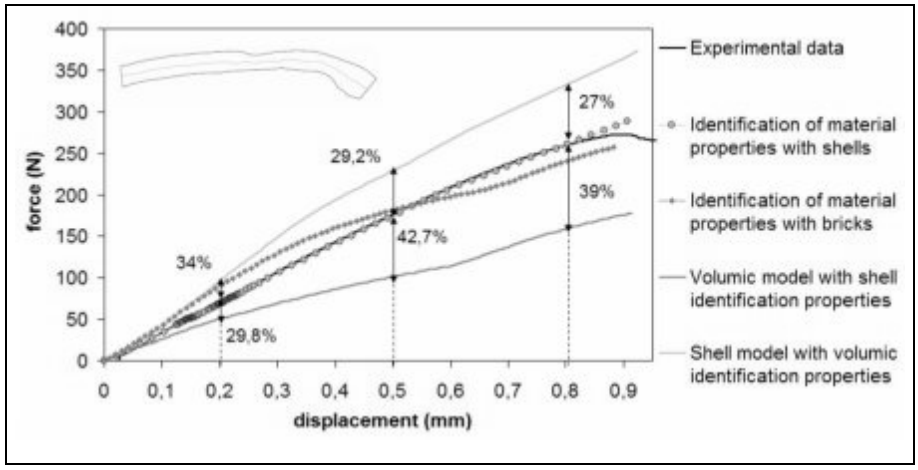

Figure 13. *Experimental and numerical force versus displacement curves for sample 2*

As observed in the simple case study, the response of the two brick finite element models presented perturbations. So, these identification results were approximate for the two samples loaded using four-point bending configuration.

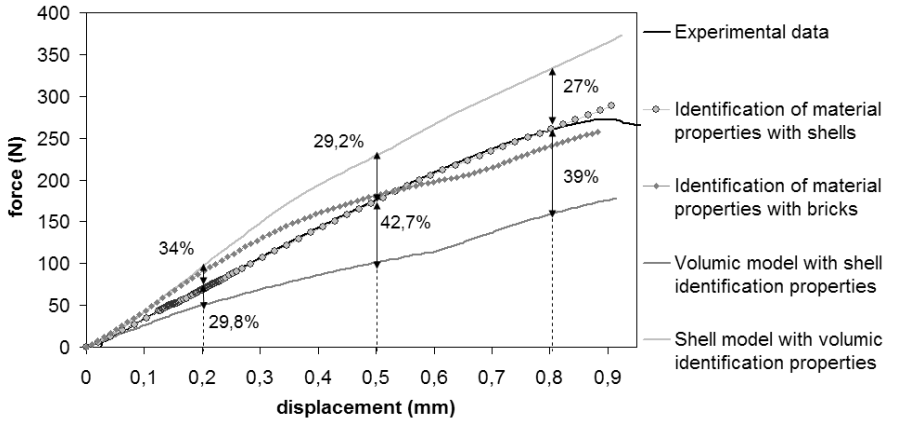

Figure 14. *Experimental and numerical force versus displacement curves for sample 3*

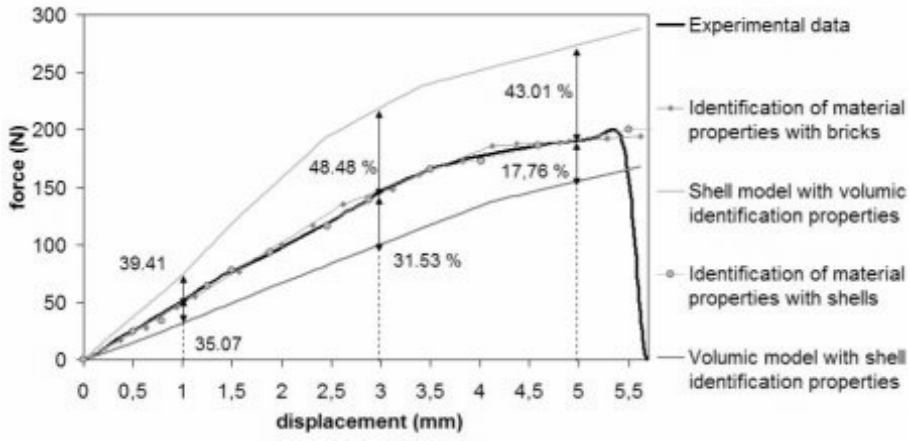

Figure 15. *Experimental and numerical force versus displacement curves for sample 4*

Stiffness difference between brick and shell elements was also observed on cantilever beam bending results (Fig.14-15). Actually, Young's modulus identified with bricks was 40% higher for sample 3 and 53% higher for sample 4 (Table 3).

Moreover, numerical curves of the two samples showed that the simulation performed using shell mesh associated to material properties identified using brick finite element model gave error values higher than the opposite configuration.

Table 3. *Numerical identification results*

Samples	Mechanical properties identified : E, σ_e, E_t (MPa)	
	Shell model	***Brick model***
1	*2600, 20, 2000*	
2	*4516, 20, 2000*	*7145, 20, 3400*
3	*2000, 20, 1700*	*2800, 27, 2195*
4	*980, 26, 636*	*1500, 55, 1000*

4. Discussion and conclusion

Experimental tests presented in this paper were performed on human bone samples among which half were taken from fresh material. Then, results may enhance significantly the existent database since most of the few studies found in the bibliography were performed on embalmed or frozen samples. Moreover, samples were non machined skull fragments and were loaded in bending configuration, which is nearest to the real loading sustained by the skull during a car crash than traction or compression loading. The use of non machined bone samples to find mechanical properties was allowed by the identification method coupled to the finite element modeling. Nevertheless, it implies instability of the sample during the four-point bending tests. Actually, the skull shape is extremely irregular and the material availability didn't allow selecting samples depending on their geometry.

Two numerical reconstruction methods were employed to realize the finite element models of bone samples. The first one was performed using a 2D scan (for sample 1 and 2) and was based on a hypothesis of geometry invariance along the transversal beam section. The shell and brick meshes then realized were geometrically equivalent since their respective mass, gravity centre location and dynamical inertia were corresponding. Thus, the manual layout of the mean surface and the shell thickness computing were efficient. However, the hypothesis chosen for this reconstruction method of these two mesh types is very simplifying. Transversal sample dimension could be minimized to reduce the curved shape but it would bring instability and may involve beam rotation during the four-point bending test. The second reconstruction method was carried out using 3D digital pointing and the brick model obtained was more accurate. On the other hand, the external surface was used as mean plane of the shell element and the thickness was measured normal to this surface. This explains the relatively important error between shell and brick meshes.

The comparison between analytical and numerical solution corresponding to simple loading cases allowed the underlining of some specific points. First, the global behaviour of samples was influenced by the element type. Actually, for the

four-point bending simulation, the shell mesh results fitted to the analytical solution whereas the brick mesh showed difference. Secondly, sample's response was influenced by the loading configuration since the results of cantilever beam loading were equivalent for the two mesh types. Finally, modelling the contact interface for the four-point bending had an instability effect on the behaviour of brick mesh, not on shell mesh (to avoid instability an artificial damping coefficient could be used).

The identification achieved using experimental bending tests and finite element simulations gave pertinent results in regard of the data found in bibliography. Actually, the mean value of Young's modulus obtained with the eight simulations is equal to 3017 MPa (max=7145 MPa). The range of values given by Hubbard was between 7791 to 15306 MPa, but the bending tests were performed on embalmed material (Hubbard, 1971). Moreover, the traction tests achieved by McElhaney on fresh material gave a mean Young's modulus equal to 5377 MPa which is quite comparable since results are influenced by biological variability (McElhaney *et al.*, 1970).

Identification results were highly influenced and biased by element type as well as loading conditions. Then, modelling the contact interface introduced instability only for the brick mesh which was submitted to four-point bending loading. Moreover, identification data also depended on the geometry reconstruction since simulation results for cantilever beam bending tests could be explained by the differences found on inertia comparison.

In conclusion, the loading type and finite element mesh must be chosen depending on samples geometry. When the available material is sufficient, samples could be selected in relation with their linear geometry, and then perform shell finite element model to reduce computational time. But when the samples present a non linear shape and the mean surface can not be reconstructed accurately, brick finite element mesh may be chosen and loaded simply (cantilever beam tests) to avoid numerical instability and high computational time. In the case of complex geometry, numerical simulation can't be performed using shell mesh and mechanical properties identified with bricks, or vice versa.

5. References

Autuori B., Bruyère-Garnier K., Morestin F., Brunet M., Verriest J.P. "Static experimental testing on facial bone and finite element modelling", *Proc. of International Crashworthiness and Design Symposium*, Lille, décembre 2003, Tome 3, p. 1197-1206.

Autuori B., Bruyère-Garnier K., Morestin F., Brunet M., Verriest J.P., "Assessment of a finite element model of the human facial bone structure", *27e Congrès de la Société de Biomécanique*, Valenciennes, septembre 2002, *Archives of physiology and biochemistry*, vol. 110, p. 36, septembre 2002.

Barber T. W., Brockway J. A., Moffatt C. A., “Static compression testing of specimens from embalmed human skull”, *Texas Report on Biology and Medicine*, vol. 28, n° 4, 1970, p. 497-508.

Canaple B., Rungen P., Drazetic P., Markiewicz E., Cesari D., “Towards a finite element head model used as a head injury predictive tool”, *Int. Journal of Crashworthiness*, vol. 8, n° 1, 2003, p. 41-52.

Crandall J.R., *The preservation of human surrogates for biomechanical studies*, University of Virginia, USA, 1994.

Delille C., Baivier S., Masson C., Drazetic P., “Identification of skull behavior laws starting from bending tests”, *Mécanique & Industries*, vol. 4, 2003, p. 119-123.

Delille C., Masson C., Drazetic P., Delille R., Markiewicz E., Canaple B. & Cesari D., “Quasi-static bending testing of specimens from embalmed human skull : experimental data”, *Archives of physiology and biochemistry*, vol. 110, 2002, p. 28.

Delille R., Delille C., Drazetic P., Masson C., Markiewicz E., Canaple B. & Cesari D., “Quasi-static bending testing of specimens from embalmed human skull : numerical phase”, *Archives of physiology and biochemistry*, vol. 110, 2002, p. 39.

Evans F. G., Lissner H. R., “Tensile and compressive strength of human parietal bone”, *J. of Appl. Physiol.*, vol. 10, n° 3, 1957, p. 493-497.

Ferre J.C., Barbin J.Y., “Réflexions sur la structure mécanique de la calvaria (voûte du crâne)”, *Orthod. Fr.*, vol. 57, n° 2, 1986, p. 729-739.

Ferre J.C., Chevalier C., Barbin J.Y., « Réflexions sur la biomécanique de la base du crâne et de la face », *Revue de Stomatol.Chir. Maxillofac.*, vol. 91, n° 1, 1990, p. 1-8.

Hubbard R. P., “Flexure of layered cranial bone”, *J. of Biomech.*, vol. 4, 1971, p. 251-263.

Journal Officiel des Communautés Européennes, 1997, Directive 96/79/CE du Parlement européen et du Conseil du 16 décembre 1996 concernant la protection des occupants des véhicules à moteur en cas de collision frontale et modifiant la directive 70/156/CEE. JO n° L 018 du 21/01/1997, p. 007-005.

King A. I., Kang K. H., Zhang L., Hardy W., “Is head injury caused by linear or angular acceleration ?”, *IRCOBI Conference*, Lisbon, Portugal, sept. 2003, p. 1-12.

Kleiven S., Von Holst H., “Consequences of head size following trauma to the human head”, *J. of Biomech.*, vol. 35, n° 2, 2002, p. 153-160.

Laumon B., Recherches coordonnées sur les traumatismes consécutifs à un accident de la circulation routière, et sur leurs causes et conséquences, Rapport n° 0206, 2 tomes, 2002, Lyon, INRETS, 292 p. et 129 p.

McElhaney J. H., Fogle J. L., Melvin J. W., Haynes R. R., Roberts V. L., Alem N. M., “Mechanical properties of cranial bone”, *J. of Biomech.*, vol. 3, 1970, p. 495-511.

Newman J., Beusenberg M., Fournier E., Shewchenko N., Withnall C., King A., Yang K., Zhang L., McElhaney J., Thibault L., McGinnis G., “A new biomechanical assessment of mild traumatic brain injury. Part I : Methodology”, *IRCOBI Conference*, Sitges, Espagne, 1999, p. 17-36.

Schueler F., Zimmer G., Min J., Mattern R., “Assessment of mechanical properties of the human skull-cap through basic biomechanical tests and quantitative computed tomography (QCT)”, *IRCOBI Conference*, Lyon, France. 1994, p. 23-37.

Willinger R., Baumgartner D., “Human head tolerance limits to specific injury mechanisms”, *Int. J. of Crashworthiness*, vol. 8, n° 6, 2003, p. 605-617.

Wood J. L., “Dynamic response of human cranial bone”, *J. of Biomech.*, vol. 4, 1971, p. 1-12.